ELSEVIER

Catalysis Today 51 (1999) 113–125

CATALYSIS TODAY

Progress in design of new amorphous alloy catalysts

Jing-Fa Deng[a,*], Hexing Li[b], Weijiang Wang[a]

[a]*Department of Chemistry, Fudan University, Shanghai 200433, China*
[b]*Department of Chemistry, Shanghai Normal University, Shanghai 200234, China*

Abstract

Three new kinds of Ni-based amorphous alloy catalysts, Raney type Ni–P(R–Ni–P), Ni–Co–B, and Ni–B(P)/SiO_2, have been prepared by modification of either the rapid quenching method or chemical reduction. Their amorphous structures have been determined by XRD, EXAFS, and DSC. Their catalytic activities and selectivities have been measured during the hydrogenation of various organic compounds, which demonstrate the great improvement on the catalytic properties in comparison with the corresponding amorphous alloy catalysts prepared by the rapid quenching method or chemical reduction previously reported. These new amorphous catalysts also exhibit superior catalytic properties over the traditional catalysts, such as Raney Ni, Ni/SiO_2, and Pd/C, making them possible to be used in real industrial catalysis. The relationship between the catalytic properties and the structural properties has been discussed according to various characterizations, including ICP, XPS, EXAFS, XRD, TPD, TPR, hydrogen adsorption, IR, SEM, and TEM, etc. The higher hydrogenation activity of R–Ni–P than the Ni–P amorphous catalyst obtained by rapid quenching is mainly ascribed to the increase of the surface area due to the skeleton structure; the higher activity of Ni–Co–B than the Ni–B amorphous catalyst demonstrates a promoting effect of the additive metal(s); while the higher thermal stability of supported Ni–P(B) than the corresponding unsupported catalysts can be explained by considering the stabilizing effect of the silica support on the amorphous structure.

Keywords: Hydrogenation; Skeletal Ni–P amorphous catalyst; Ni–Co–B amorphous catalyst; Supported Ni–P(B) amorphous catalyst

1. Introduction

Since the introduction of the rapid quenching techniques [1] for producing metallic glasses, i.e., the metal–metalloid amorphous alloys, those metastable materials with not long-range ordering but with short-range ordering structure, have attracted a lot of attention from metallurgists, physicists, engineers and material scientists owing to their superior electronic, magnetic, mechanical and chemical properties [2,3]. However, the study of heterogeneous catalysis with amorphous alloys did not come about until 1980 [4]. The classical work of Yamashita and Masumoto et al. [5–15] in the 1980s stimulated fast growth in amorphous alloy catalysis research. Various amorphous alloys have been prepared and employed in catalysis including electrolysis [16,17], hydrogenation [5–10, 18–35], hydrogenolysis [9,10], oxidation [36–40], isomerization [29,41,42], etc. Among them, the Ni-based amorphous alloys have been studied most thoroughly. The most widely used techniques for the preparation of amorphous alloy catalysts are classified into (i) the rapid quenching method, and (ii) chemical reduction. Each method has both advantages and disadvantages.

*Corresponding author.

0920-5861/99/$ – see front matter
PII: S0920-5861(99)00013-9

The rapid quenching method [1–3], which ensures a cooling rate of at least 10^5–10^6 K.s^{-1}, is the only practical way to obtain amorphous alloys in large quantities. Usually, the resultant specimens are ribbons from several millimeters to several centimeters in length. Such amorphous alloys can be produced with wide composition ranges not available in crystalline form, making it easier to adjust their electronic properties. Their single-phase character and the possible lack of surface segregation of the alloying elements ensure that the active sites are in a uniform dispersion in a homogeneously chemical environment. They also have a high concentration of coordinatively highly unsaturated sites, which makes adsorption and surface reactions easier than on the corresponding crystalline catalysts. The nonporous structures of those amorphous alloys can effectively eliminate the effects of intraparticle diffusion limitations on surface reactions. All those features make amorphous alloys attractive materials in heterogeneous catalysis. However, those amorphous alloys also have some disadvantages:

1. Special equipment is required in their preparation, which is not available in most labs.
2. Pretreatment of those amorphous alloys is necessary before a catalytic test.
3. The catalytic reactions must be performed at low temperatures to avoid the crystallization process, since the amorphous structure is thermodynamically metastable.
4. Perhaps, the most important disadvantage is the low surface area of those amorphous alloys, i.e., less than 1 m^2/g, which is too small to use as an industrial catalyst because of the low productivity per unit weight of catalyst.

Several new methods have been developed recently to prepare amorphous alloys with higher surface areas. One of the most powerful methods is to prepare the amorphous alloys by chemical reduction of the metallic ions with hypophosphite ($H_2PO_2^-$) or borohydride (BH_4^-) to form ultrafine metal boride or phosphide amorphous alloy particles, as first reported by van Wonterghem et al. in 1986 [43] and developed by Linderoth and Morup et al. [44–50]. Chemical reduction ensures large surface areas of the resultant amorphous alloy catalysts, e.g., the ultrafine Ni–B amorphous alloy obtained by chemical reduction in ethanol solution has a surface area of up to 200 m^2/g [23]. Experimental results demonstrate that their catalytic activities are usually 50–100 times higher than those of the corresponding amorphous alloys obtained by the rapid quenching method. These amorphous alloy particles can be compacted in a variety of forms suitable for catalysis and can be used in catalytic test without any pretreatment, which makes them more convenient in catalytic studies. In addition, the simple preparation procedure of these amorphous alloys makes it possible that they are studied widely in many labs. However, they also have some drawbacks. One is that the storage of these amorphous alloys is difficult, since they are easily oxidized by air. Another one is that these amorphous alloys are costly in comparison with those obtained by the rapid quenching method. Perhaps, the extremely poor thermal stability of these amorphous alloys due to the high surface energies of the ultrafine particles is the most important factor limiting their application in industrial processes.

Due to their drawbacks as mentioned above, no industrially used amorphous alloy catalysts have been reported so far. Therefore, modification of the present techniques seems essential to prepare amorphous alloy catalysts which can be used in industrial processes. This paper is a brief summary of our research work on the design of new amorphous alloy catalysts with the aim of making them suitable for real industrial processes. In Section 2, we describe the preparation and the characterization of three new kinds of as-prepared Ni-based amorphous catalysts. In Section 3, we describe their catalytic properties and the potential application during the hydrogenation of various organic compounds, such as benzene, nitrobenzene, cyclopentadiene and 4-carboxyl benzaldehyde, etc. The relationship between the catalytic properties and the surface structural properties is discussed, in which emphasis is placed on the stabilizing effect of the silica support on the Ni–P amorphous structure and the promoting effect of Co in Ni–Co–B amorphous catalysts.

2. Preparation and characterization of the supported amorphous alloy catalysts

2.1. Preparation methods

A. R–Ni–P amorphous alloy catalyst. A R–Ni–P amorphous alloy catalyst is prepared by the following

procedure [51]: A Ni–Al–P amorphous alloy with 48.2 wt% Ni, 48.7 wt% Al and 3.1 wt% P, in the form of ribbons ca. 5 mm wide and 10–20 μm thick, was prepared by the rapid quenching method using a single steel roll. The sample is ground to 200 mesh and very slowly added into 6.0 M NaOH at 273 K, in which the Al is dissolved by forming $NaAlO_2$. The alkali leaching is continued by stirring at 343 K for 6.0 h in a N_2 atmosphere. The resultant amorphous R–Ni–P catalyst is washed free from alkali and aluminate with distilled water until pH=7. It is further washed with ethanol(EtOH) to remove water, and finally, kept in EtOH. For comparison, a Raney Ni catalyst is also prepared in the same way by alkali leaching of a commercial Ni–Al alloy (Ni/Al 50/50 w/w). A regular Ni–P amorphous alloy is obtained by the rapid quench method as described elsewhere [5,6].

B. Supported Ni–B(P) amorphous alloy catalysts. A Ni–P/SiO_2 amorphous catalyst is prepared by the following procedures [52,53]: 1.0 g SiO_2 (198 m^2/g, 40–60 mesh) is impregnated overnight with an aqueous $NiCl_2$ solution containing 0.010 g nickel. After being dried at 373 K and further calcined at 623 K for 2.0 h, the Ni^{2+} on the support is reduced by an alkaline NaH_2PO_2 solution (pH=11) at 363 K to create nuclei on the support. After being washed thoroughly with distilled water, the sample is transferred to a plating solution containing 10.0 g/l each of $NiCl_2{\cdot}6H_2O$, $NaH_2PO_2{\cdot}6H_2O$, CH_3COONa and sodium citrate, for electroless plating. During reaction, the mixture is stirred vigorously at 363 K. The plating process is continued for about 2.0 h until no significant bubbles release from the solution. The resulting Ni–P/SiO_2 amorphous catalyst with a nickel loading of ca. 5 wt% is then washed thoroughly with distilled water and ethanol. Finally, it is stored in EtOH. The loading of the Ni–P alloy on the support can be adjusted easily by changing the concentration of the plating solution.

A Ni–B/SiO_2 amorphous catalyst is prepared by impregnating overnight a silica support with an aqueous $NiCl_2$ solution containing the desired amount of nickel. After being dried at 373 K, it is reduced by adding a KBH_4 solution dropwise at room temperature. The resulting Ni–B/SiO_2 amorphous catalyst is then washed thoroughly with water and EtOH. Finally, it is kept in EtOH.

C. Ultrafine Ni–Co–B amorphous alloy catalysts. An ultrafine Ni–Co–B amorphous alloy catalyst is prepared as reported previously [21,22]. An aqueous solution of KBH_4 (2.0 M) is added dropwise to an aqueous solution containing both nickel acetate and cobalt acetate. The initial molar ratio of KBH_4 to metallic salts is 5:2 to ensure complete reduction of metallic ions in the solution. The solution is kept in an ice water bath and stirred vigorously by a magnetic stirrer. The reaction is continued for about 0.5 h until no more gas is released. The resulting black precipitate is washed several times with distilled water and subsequently with 99.9% ethanol (EtOH). The final product is kept in EtOH. The composition of the samples is adjusted by changing the initial Ni/Co ratio in the solution. In the extreme, Ni–B and Co–B amorphous alloys are obtained when single nickel salt or cobalt salt is used in the solution, respectively.

2.2. Characterization

2.2.1. Amorphous structure

XRD, EXAFS and DSC are used to determine the amorphous structure of the as-prepared samples. Sometimes, selected area electronic diffraction (SAED) is also employed. Fig. 1 shows the XRD patterns of the as-prepared R–Ni–P, Ni–Co–B, Ni–P/SiO_2, and Ni–B/SiO_2 samples. By subtracting a broad peak around 22° resulting from the amorphous silica support, the only other broad peak around 45° appeared on the XRD pattern of each of these samples demonstrates the typical amorphous structures [5]. After treatment at high temperature, the various sharp peaks appearing in the XRD patterns of these samples indicate the occurrence of crystallization, as found in Ni–P/SiO_2 [54]. The amorphous structure of the as-prepared samples can be further characterized by EXAFS spectra, from which the radial distribution function (RDF) curves can be obtained. A typical result of the as-prepared Ni–P/SiO_2 fresh sample and the corresponding one after treatment at 873 K in N_2 flow for 2.0 h is shown in Fig. 2. The strength of the RDF peaks refers to the degree of the ordering structure, while the number of the RDF peaks refers to the range of the ordering structure. For the fresh sample, only one RDF peak is observed, suggesting that the sample has only a short-range ordering structure confined to the first coordination shell. For the same sample after treatment at high temperature, both the intensity and the number of the RDF peaks

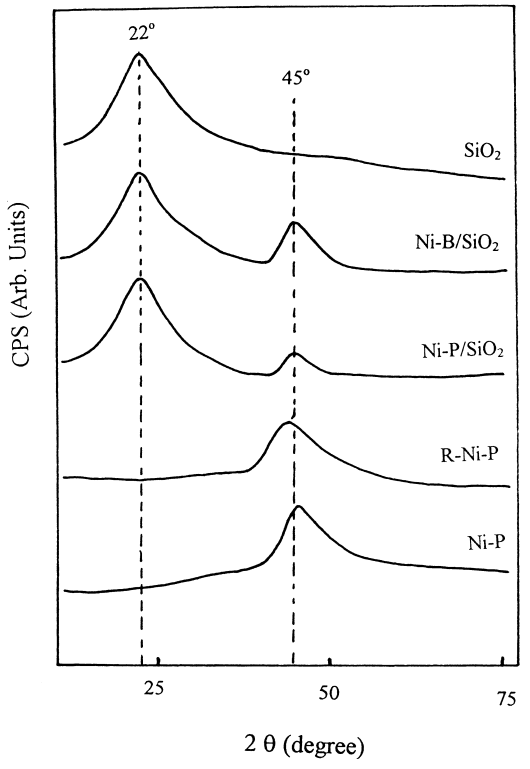

Fig. 1. XRD patterns of the as-prepared amorphous alloy catalysts.

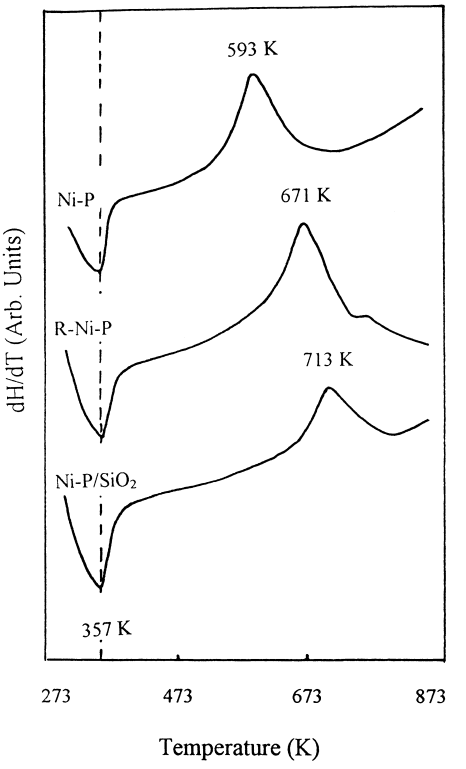

Fig. 3. DSC curves of the as-prepared amorphous alloy catalysts.

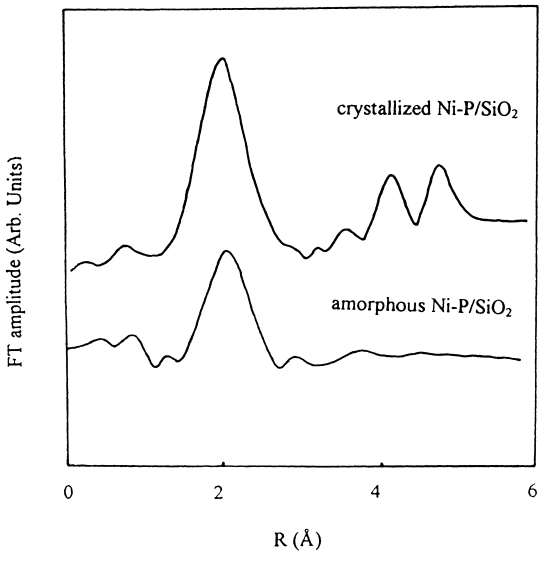

Fig. 2. RDF curves of amorphous and crystallized Ni–P/SiO_2.

increased, indicating the occurrence of crystallization. The transformation of the amorphous structure during the heating treatment can also be followed by a DSC measurement. Typical results of the DSC curves of the Ni–P, R–Ni–P and Ni–P/SiO_2 samples are shown in Fig. 3. The first endothermic peak is attributed to the loss of the solvent absorbed by the catalyst. The other exothermic peaks are attributed to the transformation from an amorphous to a crystalline structure. Commonly, the temperature corresponding to the first exothermic peak in a DSC curve is defined as the crystallization temperature (T_c). The higher T_c of R–Ni–P as well as Ni–P/SiO_2 than Ni–P indicates the promoting effect of the skeleton structure or the silica support on the thermal stability of the amorphous structure. The stabilizing effect of the support will be discussed in the following section.

2.2.2. *Surface morphology*

The surface morphologies of both the supported and unsupported amorphous alloy catalysts are determined

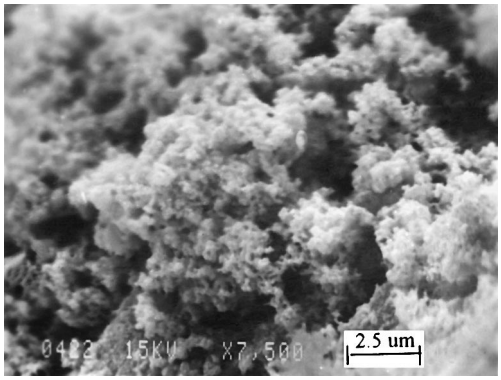

Fig. 4. SEM morphology of Ni–P/SiO_2 amorphous alloy catalyst.

by SEM and TEM. A typical SEM picture of the as-prepared Ni–P/SiO_2 amorphous catalyst is shown in Fig. 4, which shows that the support is covered by the cotton like Ni–P alloy clusters comprising thousands of small particles. These particles are spherical in shape with an average size between 50 and 100 nm, as determined by TEM in Fig. 5.

2.2.3. Surface electronic state

XPS measurements are employed to analyze both the surface compositions and the surface electronic states of the as-prepared supported amorphous catalysts. A typical result of the Ni–P/SiO_2 amorphous alloys is shown in Fig. 6, in which one can see that the surface nickel exists in the elemental as well as in the oxidized state, while phosphorus is only present in its elemental state. In comparison with the standard

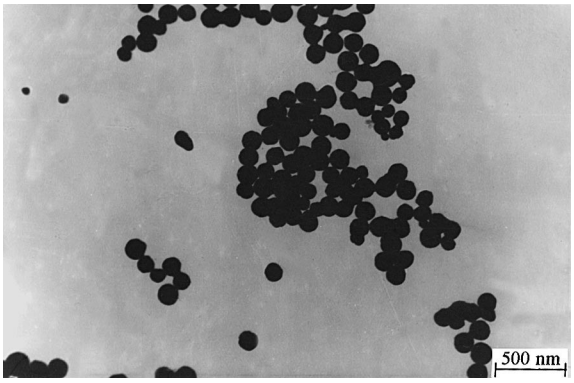

Fig. 5. TEM morphology of Ni–P amorphous alloy catalyst.

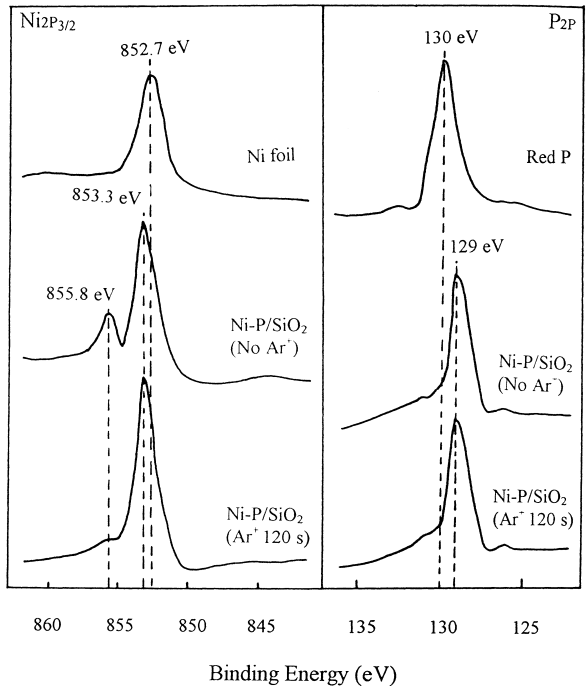

Fig. 6. XPS spectra of metallic nickel foil, red phosphorus, and Ni–P amorphous alloy catalyst.

binding energies of the metallic Ni foil and red phosphorus, the positive shift of the binding energy corresponding to elemental Ni and the negative shift of the binding energy corresponding to elemental P in the Ni–P/SiO_2 sample indicated the electron transfer from Ni to P. With Ar^+ sputtering, one can observe the change of the surface composition with depth. The results show the enrichment of P on the top surface of the catalyst. It is also found that the content of the oxidative Ni decreases while the content of the elemental Ni increases with the increase of the Ar^+ sputtering time, indicating the occurrence of surface oxidation of metallic Ni by air during the preparation and pretreatment of the Ni–P/SiO_2 amorphous catalyst.

2.2.4. Other characterizations

The bulk compositions and the contents of the amorphous alloys on the support are determined by ICP. Their surface areas are determined by both BET method (S_{BET}) and hydrogen chemisorption (S_{active}). The interactions between the amorphous alloys and the support are investigated by XPS, IR and Raman

Table 1
Properties of the as-prepared supported Ni-based amorphous catalysts

Samples	Ni loading (wt%)[a]	Composition (atomic ratio)	S_{BET} (m^2/g)	S_{Ni} (m^2/g)	T_c (K)
Ni–P	–	$Ni_{88}P_{12}$	1.2	0.8	593
R–Ni–P	–	$Ni_{68}Al_{25}P_{14}$	87	38	671
Ni–P/SiO_2	3.0	$Ni_{86}P_{14}$	187	25.0	713
Ni–B/SiO_2	10.0	$Ni_{76}B_{24}$	156	22.5	610
Ni–Co–B	–	$Ni_{32}Co_{32}P_{36}$	7.5	6.8	653

[a] Weight percentage.

spectroscopy. The surface hydrogen adsorption and desorption are determined by TPR and TPD. Some properties of Ni–P, R–Ni–P, Ni–Co–B, and Ni–P/SiO_2 amorphous alloy catalysts are summarized in Table 1.

3. Activity test

3.1. R–Ni–P amorphous catalyst

The liquid phase hydrogenation of various organic compounds, including benzene, toluene, and hexanedinitrile, is employed to evaluate the catalytic activity and selectivity of the as-prepared R–Ni–P amorphous alloy catalyst. A typical result of liquid phase hexanedinitrile hydrogenation to 1,6-hexanediamine, which is an important intermediate in the production of nylon-6,6, is summarized in Fig. 7. It is found that both the TOF value and selectivity of R–Ni–P are almost the same as those of Ni–P owing to their similar amorphous structures. However, the activity of R–Ni–P is about 50 times higher than that of Ni–P. This can be ascribed to the significantly higher surface area, as shown in Table 1. In comparison with Raney Ni, which is most widely used in the above hydrogenation reaction, the R–Ni–P catalyst exhibits an increase of about 2–3 times in activity and about 40% in selectivity, showing the potential of the R–Ni–P amorphous catalyst instead of Raney Ni in industrial processes. The better selectivity of R–Ni–P is mainly attributed to the promoting effect of its amorphous structure [2,3]. The higher hydrogenation activity and TOF value of R–Ni–P compared to Raney Ni can be understood by considering the promoting effects of both the amorphous structure and the alloying of phosphorus in the R–Ni–P catalyst. XRD and EXAFS show the shorter Ni–Ni bond length and more highly unsaturated sites in the R–Ni–P catalyst in comparison with the Raney Ni catalyst. TPD and SEM as well as EXAFS reveal that only one kind of active sites are present in the as-prepared R–Ni–P amorphous alloy catalyst which are homogeneously dispersed on the catalyst surface. These factors are claimed favorable for hydrogenation [2,3,25,55]. In comparison with pure metal Ni and red P, as shown in Fig. 6 XPS spectra reveal that a partial electron transfers from Ni to P, making Ni electron-deficient, which is also favorable for the hydrogen adsorption and the hydrogenation on the surface of Ni active sites [12,56–58].

3.2. Ni–Co–B

The dependence of the hydrogen uptake rate per gram of Ni–Co–B amorphous alloy catalyst

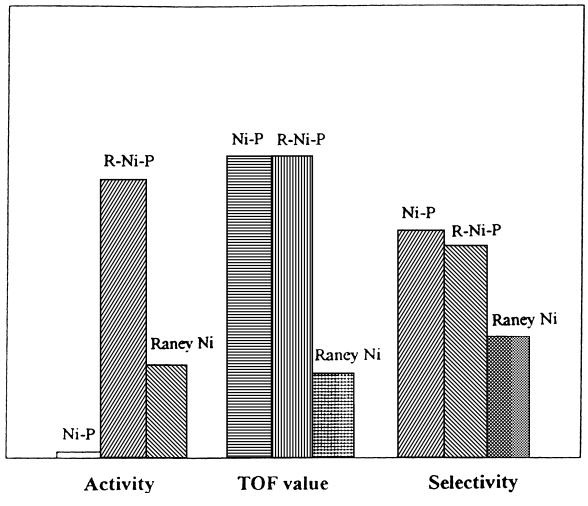

Fig. 7. Catalytic activity (mmol $H_2/h \cdot g_{Ni}$), selectivity, and TOF value of the as-prepared R–Ni–P and Ni–P amorphous alloy catalysts as well as Raney Ni during the liquid phase hydrogenation of hexanedinitrile (HDN) to 1,6-hexanediamine. Reaction conditions: T=350 K, P_{H_2}=4.0 MPa, EtOH/HDN (v/v)=3:1.

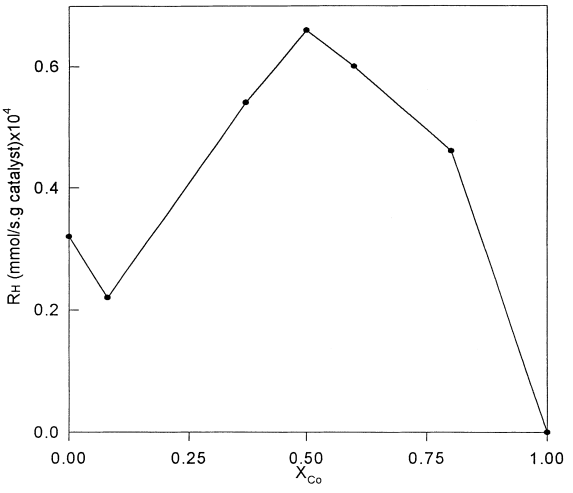

Fig. 8. Dependence of catalytic activity of Ni–Co–B amorphous alloy catalysts on the Co content in the Ni–Co alloy during liquid phase benzene hydrogenation. Reaction conditions: T=373 K, P_{H_2}=1.0 MPa, EtOH/benzene (v/v)=4:1.

(R_H mmol/s·$g_{catalyst}$) on the molar ratio of Co in the Ni–Co alloy (χ_{Co}) during the liquid benzene hydrogenation is shown in Fig. 8 [22]. According to the BET test, the total surface areas of all these Ni–Co–B samples are around 12.0 m^2/g, indicating that the effect of χ_{Co} on the catalyst dispersion is very little. So the change of the specific hydrogen uptake rate over the unit surface area of Ni–Co–B amorphous alloy catalysts with χ_{Co} is in the same way as that of the R_H. Because no significant activity of the Co–B amorphous alloy is observed, the higher activity of Ni–Co–B than Ni–B amorphous alloy catalyst indicates a promoting effect of the Co on the hydrogenation activity. Since XPS spectra show almost the same binding energy of the elemental Ni in the Ni–B as those in the Ni–Co–B with different χ_{Co}, the modification of Co additive on the electronic structure of surface Ni could be neglected. Therefore, only the structural modification is responsible for the promotion of Co on the hydrogenation activity. On one hand, the XPS spectra and hydrogen chemisorption reveal that the addition of Co to Ni–B amorphous alloy results in the increase of surface Ni atoms, which enhance the hydrogenation activity per unit weight of catalyst since only Ni atoms serve as active sites. On the other hand, as reported by Shen et al. [55] from an EXAFS experiment, the addition of Co to the Ni–B alloy results in the decrease of the Ni–Ni bond length, indicating an increase in the Ni–Ni interaction. They also found that the structural disordering extent factor (σ) increased with the addition of Co, corresponding to a more homogeneous distribution of the active sites. These results also account for the promoting effect of Co on the hydrogenation activity [3]. The change of R_H with the χ_{Co} in Fig. 8 could be explained as follows. On one hand, the increase of Co content (χ_{Co}) will increase the hydrogenation activity due to its promoting effect as mentioned above. On the other hand, the increase of χ_{Co} will decrease the Ni content per unit weight of the Ni–Co–B alloy, resulting in a decrease of the hydrogenation activity since only Ni atoms serve as the catalytic active centers in the catalyst. In the beginning, since no significant decrease of Ni content occurs, the promoting effect of the Co is dominant, therefore, R_H increases with χ_{Co}. When χ_{Co} is high enough, the decrease of Ni content per unit weight of the Ni–Co–B alloy becomes dominant, resulting in a decrease of R_H with χ_{Co}, as shown in Fig. 8. The optimum Ni/Co molar ratio is determined as 1:1.

3.3. *Ni–B/SiO_2 amorphous catalyst*

Tables 2 and 3 show the application of the Ni–B/SiO_2 amorphous catalyst in the selective hydrogena-

Table 2
Selective hydrogenation of cyclopentadiene (CPD) to cyclopentene (CPE) at normal pressure and 393 K in a fixed bed

Catalyst	H_2:CPD (molar ratio)	LHSV[a] (1/h)	Conversion (%)	Selectivity (%)	Lifetime (h)
5%Ni–B/SiO_2	1.4	12	100	96	>1000
5%Ni/SiO_2	2.0	12	100	80	–
5%Ni/Al_2O_3	2.0	12	100	50	–
0.5% Pd/C	3.0	2	<100	45	–

[a] Liquid velocity.

Table 3
Benzene hydrogenation at normal pressure in a fixed bed

Catalyst	LHSV[a] (1/h)	H_2:benzene	T (K)	Solvent	Conversion (%)	Selectivity (%)	Sulfur resistance (ppm)
15% NiB/SiO_2	2–3	2–3	423	Benzene	100	100	2000
15% Ni/SiO_2	2–3	2–3	423	Benzene	85	100	500

[a] Liquid velocity.

tion of cyclopentadiene to cyclopentene and the hydrogenation of benzene to cyclohexane in a fixed bed at atmospheric pressure [59–61]. These results show higher catalytic activities and selectivities as well as longer lifetime of the Ni–B/SiO_2 amorphous catalyst than the corresponding Ni/SiO_2 catalyst obtained by H_2 reduction at 723 K. In addition, the Ni–B/SiO_2 amorphous catalyst exhibits higher sulfur resistance than the corresponding Ni/SiO_2 catalyst since the lifetime of the Ni–B/SiO_2 amorphous catalyst is much longer than that of the Ni/SiO_2 catalyst when the same content of CS_2 is introduced in the feed gas [62]. The good catalytic activity and selectivity of the Ni–B/SiO_2 amorphous catalyst are mainly attributed to the promoting effects of its amorphous structure, just as that of the unsupported Ni–B amorphous alloy catalysts as discussed elsewhere [2,3,23,24]. The excellent sulfur resistance of the Ni–B amorphous alloy is mainly attributed to the surface electronic states of Ni–B alloy [62]. According to the XPS spectra, partial electron transfer from elemental B to elemental Ni occurs, making Ni electron-rich and B electron-deficient [6,59,63,64]. Therefore, sulfur will be adsorbed reversibly by B prior to Ni, as shown in Fig. 9, which can protect Ni from sulfur poisoning, accounting for the superior sulfur resistance of the Ni–B/SiO_2 amorphous catalyst over the corresponding Ni/SiO_2. Such a conclusion is strongly supported by the fact that no significant improvement in the sulfur resistance occurs by forming Ni–P amorphous alloy since the elemental Ni is electron-deficient in the Ni–P amorphous alloy owing to the partial electron transfer from Ni to P, as shown in Fig. 9.

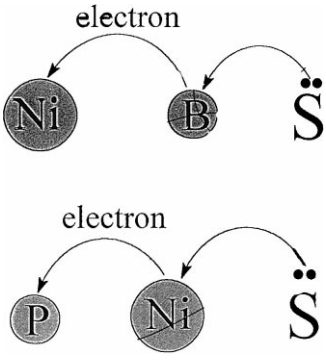

Fig. 9. Transfer of electrons and the sulfur adsorption.

In the liquid phase hydrogenation of nitrobenzene to aniline, the Ni–B/SiO_2 amorphous catalyst also exhibits superior catalytic activity over the corresponding Ni/SiO_2 catalyst [65], as shown in Table 4. The hydrogenation activity of Ni/SiO_2 decreases rapidly due to the strong adsorption of the resultant amine on the metallic Ni. However, no significant decrease in the activity of Ni–B/SiO_2 amorphous catalyst is observed owing to the presence of alloying B which protects the Ni active sites from amine poison, as mentioned in the discussion of sulfur poison.

3.4. Ni–P/SiO_2 amorphous catalyst

Terephthalic acid (TA) is an important raw material in polyester fiber production. In industry, it is obtained by oxidation of *p*-xylene, in which the 4-carboxyl

Table 4
Liquid phase hydrogenation of nitrobenzene to aniline at 1.0 MPa and 383 K

Catalyst	Solvent	R_H^{Ni} (mmol/h g)	Conversion[a] (%)	Selectivity (%)
10% NiB/SiO_2	EtOH (1:3)	174.5	18.5	98
10% Ni/SiO_2	EtOH (1:3)	61.0	4.6	76

[a] 1.0 h.

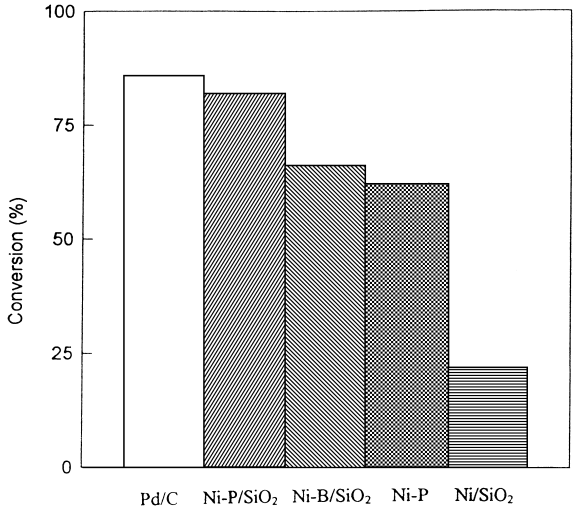

Fig. 10. The conversion of 4-carboxyl benzaldehyde (4CBA) over different catalysts in liquid phase hydrogenation. Reaction conditions: T=551 K, P_{H_2}=6.8 MPa, 4CBA/TA (w/w)=2000 ppm.

benzaldehyde (4CBA) is a main side-product. Since trace 4CBA is harmful to the quality of the polyester fiber, it must be removed beyond 25 ppm. Commonly, 4CBA is removed by the liquid phase hydrogenation over a Pd/C catalyst at high pressure and temperature in which the resulted *p*-toluic acid can be separated from TA due to their different solubility in water [66]. The Ni–P/SiO_2 amorphous catalyst can be employed as a catalyst instead of Pd/C in hydrogenation of 4CBA under the same reaction conditions. The results are summarized in Fig. 10. Since the hydrogenation has to be performed at high temperature (551 K), the application of most unsupported Ni-based amorphous catalysts and even the supported Ni–B amorphous catalyst are limited due to their poor thermal stability. XRD experiments show the occurrence of severe crystallization of those unsupported Ni–P, Ni–B and supported Ni–B/SiO_2 amorphous catalysts after hydrogenation for 3.0 h, resulting in an abrupt decrease in their hydrogenation activities [54]. However, no significant crystallization is observed for the Ni–P/SiO_2 amorphous catalyst, which ensures the repetitive use of the catalyst during the above hydrogenation. Its catalytic activity is almost the same as that of Pd/C, which makes it possible to be used as a cheap catalyst instead of Pd/C in industrial TA refine.

Table 5
Properties of Ni–P/SiO_2 samples with different Ni loadings

Catalyst	Composition	Ni Loading (wt%)	Dispersion (%)	T_c (K)
Ni–P-1/SiO_2	$Ni_{86}P_{14}$	3.0	4.0	713
Ni–P-2/SiO_2	$Ni_{86}P_{14}$	5.2	3.0	673
Ni–P-3/SiO_2	$Ni_{86}P_{14}$	12.2	1.2	623
Ni–P	$Ni_{87}P_{13}$	∞	–	558

The higher thermal stability of the Ni–P/SiO_2 amorphous catalyst than that of the Ni–B/SiO_2 amorphous catalyst may be attributed to the higher crystallization temperature of the Ni–P amorphous alloy than that of Ni–B [23]. While the higher thermal stability of Ni–P/SiO_2 than that of the unsupported Ni–P is mainly attributed to the high dispersion of the Ni–P alloy particles on the support and a strong interaction between Ni–P alloy and the silica support. The details are as follows:

1. *The high dispersion of the Ni–P alloy on the support*. The crystallization temperatures (T_c) of Ni–P/SiO_2 amorphous alloy catalysts with different Ni loadings are determined by DSC analysis. The Ni loadings are analyzed by ICP. In an unsupported Ni–P amorphous alloy catalyst, its Ni loading is considered as ∞, since no support exists. The dispersion of Ni on the surface of Ni–P alloy are determined by hydrogen chemisorption. These results are summarized in Table 5, from which, one can see that the thermal stability of Ni–P/SiO_2 amorphous catalysts decreases with increasing Ni loading. Since the dispersion of the Ni–P/SiO_2 amorphous alloy catalysts also decreases with increasing Ni loading, one can conclude that the higher the dispersion, the higher the thermal stability.
2. *The strong interaction between the Ni–P alloy and the support*. Fig. 11 shows the IR spectra of fresh silica and the Ni–P/SiO_2 amorphous catalyst with a Ni loading of 3 wt%. The IR spectrum of the fresh silica support displays two bands due to ν_{as}Si–O and ν_sSi–O at 1096 and 802 cm^{-1}, respectively [67]. For the Ni–P/SiO_2, the significant decrease in the strength of those two bands and the appearance of a new band at 660 cm^{-1} strongly demonstrate

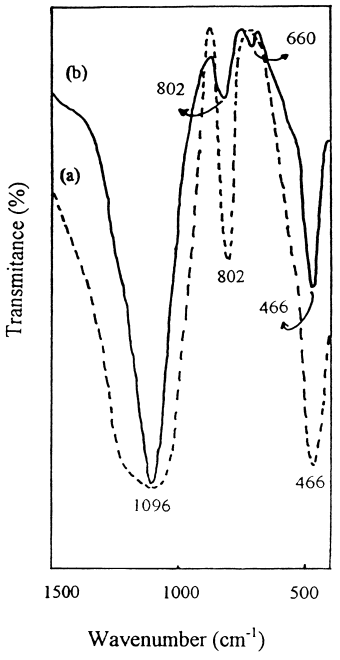

Fig. 11. IR spectra of (a) SiO_2 and (b) Ni–P/SiO_2.

the interaction between the Ni–P alloy and the silica support. Additional evidence for the strong interaction between Ni–P alloy and silica support is obtained from DSC spectra of Ni–P/SiO_2 amorphous alloy catalyst and its corresponding unsupported Ni–P amorphous alloy obtained at the same conditions, as shown in Fig. 3. The higher crystallization temperature of Ni–P/SiO_2 sample than that of Ni–P sample indicates the stabilizing effect of the silica support on the Ni–P amorphous structure. In addition, TPO experiment also demonstrates the stabilizing effect of the silica support on the elemental Ni since no significant oxidation of the Ni–P/SiO_2 amorphous alloy catalyst occurs until 623 K, while the corresponding unsupported Ni–P sample can be oxidized with sparkle even at room temperature. A model of the interaction between Ni metal and silica support is recently proposed by Ghuge et al. [67].

In order to understand the stabilizing effect of the support on the amorphous structure, the crystallization process of the Ni–P amorphous alloy is studied by XRD and SEM during its heating pretreatment

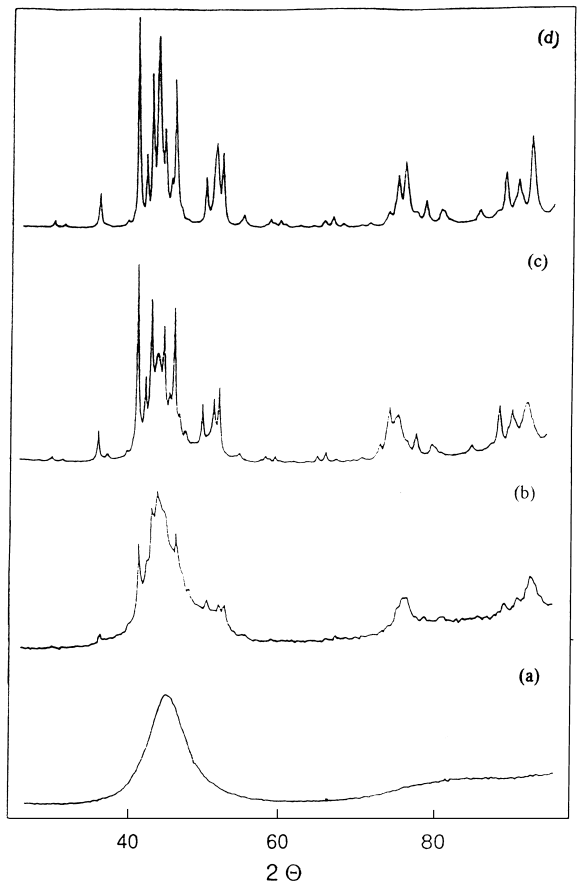

Fig. 12. XRD patterns of a Ni–P amorphous alloy film treated at different temperatures for 2.0 h (a) room temperature, (b) 580, (c) 590, and (d) 610 K.

[68,69]. From the XRD patterns in Fig. 12, one can observe that the amorphous Ni–P alloy gradually separates into two crystalline phases, Ni and Ni_3P. During the crystallization process, the gathering of the small Ni–P alloy particles and the rearrangement of the Ni–P alloy are also determined by SEM, as shown in Fig. 13. These results demonstrate that diffusion and the migration of the composition elements in Ni–P amorphous alloy are essential during its crystallization process. Therefore, the thermal stability of the Ni–P amorphous alloy is greatly improved by the silica support owing to the effective inhibition of the above diffusion and migration because of the high dispersion of Ni–P alloy on the support and the strong interaction between the Ni–P alloy and the silica support.

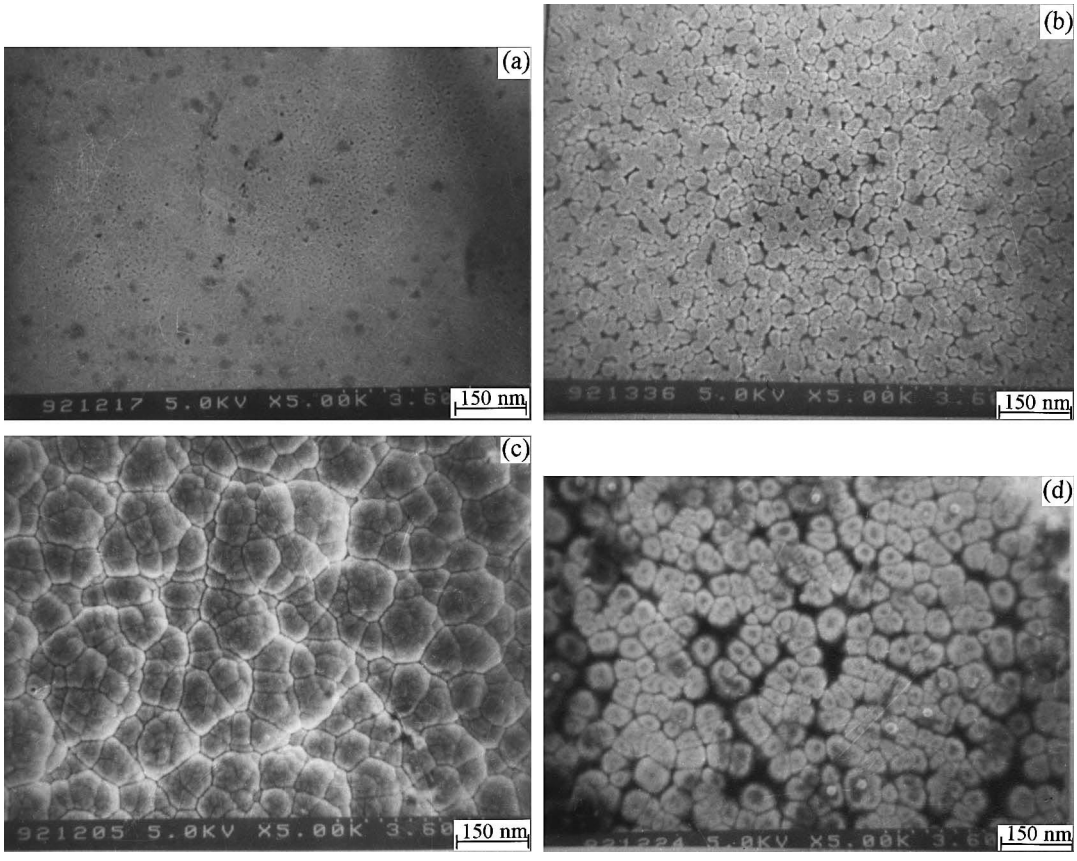

Fig. 13. SEM morphologies of a silicon supported Ni–P amorphous alloy treated at different temperatures for 2.0 h (a) room temperature, (b) 580, (c) 590, and (d) 610 K.

4. General summary

Three kinds of supported Ni-based amorphous alloy catalysts are prepared by modification of either the rapid quenching method or the chemical reduction method. These new amorphous catalysts exhibit higher catalytic activities and selectivities as well as better sulfur and amine resistance than the corresponding supported Ni catalysts obtained by hydrogen reduction, which can be explained by the alloying effect of the metalloids B or P on the surface electronic states and the surface structural properties. In comparison with the corresponding unsupported Ni-based amorphous alloy catalysts, the supported ones exhibit superior thermal stability during hydrogenation, owing to the stabilizing effect of the support on the amorphous structure. Addition of another transition metal to the Ni–B amorphous alloy to form a bimetallic amorphous alloy (Ni–Co–B) shows a significant enhancement in the catalytic activity owing to modification of the surface composition and surface structural properties by the additive metallic promoter. Those results are exciting because they supply promising ways to use amorphous alloy catalysts in real industrial processes. According to these modified methods, various new and powerful amorphous alloy catalysts, such as Raney Ni–Co–P, Raney Ni–Cu–P, Raney Ni–W–P, unsupported and supported Ni–Pd–B, Ni–Co–B [70], and Ni–Co–W–B [71] can be designed which are suitable for various heterogeneous catalytic reactions. Before these new amorphous alloy catalysts can be utilized in real industrial processes, chemical

engineering studies must be conducted and suitable reactor design must be optimized. Such studies are being considered in the future.

Acknowledgements

This work was supported by the National Natural Science Foundation of China. We are also grateful to SINOPEC for providing financial support for this study.

References

[1] K. Klement Jr., R.H. Willens, P. Duwez, Nature (London) 187 (1960) 869.
[2] M. Shibata, T. Masumoto, Prep. Catal. 4 (1987) 353.
[3] A. Molnar, G.V. Smith, M. Bartok, Adv. Catal. 36 (1989) 329.
[4] G.V. Smith, W.E. Brower, M.S. Matyjaszczyk, Proceedings of the Seventh International Congress on Catalysis, 1980, p. 355.
[5] S. Yoshida, H. Yamashita, T. Funabiki, T. Yonezawa, J. Chem. Soc., Chem. Commun. (1982) 964.
[6] S. Yoshida, H. Yamashita, T. Funabiki, T. Yonezawa, J. Chem. Soc., Faraday Trans I 80 (1984) 1435.
[7] H. Yamashita, M. Yoshikawa, T. Funabiki, S. Yoshida, J. Chem. Soc., Faraday Trans I 81 (1981) 2485.
[8] H. Yamashita, T. Faminade, T. Funabiki, S. Yoshida, J. Mater. Sci. Lett. 4 (1985) 1241.
[9] H. Yamashita, M. Yoshikawa, T. Funabiki, S. Yoshida, J. Chem. Soc., Faraday Trans I 82 (1986) 1771.
[10] H. Yamashita, T. Funabiki, S. Yoshida, J. Chem. Soc., Chem. Commun. (1984) 868.
[11] S. Yoshida, H. Yamashita, T. Funabiki, Hyomen 24 (1986) 349.
[12] H. Yamashita, M. Yoshikawa, T. Funabiki, S. Yoshida, J. Catal. 99 (1986) 375.
[13] M. Shibata, Y. Ohbayashi, N. Kawata, T. Masumoto, K. Aoki, J. Catal. 96 (1985) 296.
[14] A. Yokoyama, H. Komiyama, H. Inoue, T. Masumoto, H.M. Kimura, J. Catal. 68 (1981) 355.
[15] A. Yokoyama, H. Komiyama, H. Inoue, T. Masumoto, H.M. Kimura, J. Chem. Soc. Jpn. 2 (1982) 199.
[16] M.M. Jaksic, Electrochim. Acta 29 (1984) 1539.
[17] M.M. Jaksic, J. Mol. Catal. 38 (1986) 161.
[18] J.F. Deng, H.Y. Chen, X.H. Bao, M. Muhler, Appl. Surf. Sci. 81 (1994) 341.
[19] J.F. Deng, H.Y. Chen, J. Mater. Sci. Lett. 12 (1993) 1508.
[20] J. Chen, G. Lu, L. Ma, Fudan Univ. Acta 28 (1989) 78.
[21] H.M. Wang, Z.B. Yu, H.Y. Chen, J. Yang, J.F. Deng, Appl. Catal. A 129 (1995) L143.
[22] Z.B. Yu, M.H. Qiao, H.X. Li, J.F. Deng, Appl. Catal. A 163 (1997) 1.
[23] J. Yang, Ph.D. Dissertation, Fudan University, (1993).
[24] H.Y. Chen, Ph.D. Dissertation, Fudan University, (1994).
[25] J.F. Deng, J. Yang, S. Sheng, J. Catal. 150 (1994) 434.
[26] Z. Hu, J. Shen, Y. Chen, M. Lu, Y.F. Hsia, J. Non-Cryst. Solids 159 (1993) 88.
[27] G. Carturan, G. Cocco, E. Baratter, G. Navazio, C. Antonione, J. Catal. 90 (1984) 178.
[28] A. Baiker, H. Baeis, H.J. Guntherodt, Appl. Catal. 22 (1986) 389.
[29] W.E. Beower, M.S. Matyjaszczyk, T.L. Pettit, G.V. Smith, Nature (London) 301 (1983) 497.
[30] A. Molnar, G.V. Smith, M. Bartok, J. Catal. 101 (1986) 540.
[31] A. Molnar, G.V. Smith, M. Bartok, J. Catal. 101 (1986) 67.
[32] R. Haurert, P. Oelhafen, R. Schlogl, H.-J. Guntherodt, Solid State Commun. 55 (1985) 583.
[33] M. Funakoshi, H. Komiyama, H. Inoue, Chem. Lett. (1985) 245.
[34] A. Baiker, H. Baeis, H.J. Guntherodt, Chem. Commun. (1986) 930.
[35] C.S. Brooks, F.D. Lemkey, G.S. Golden, Mater. Res. Soc. Symp. Proc. 8 (1982) 397.
[36] K. Machida, M. Enyo, Chem. Lett. (1985) 75.
[37] K. Machida, M. Enyo, Bull. Chem. Soc. Jpn. 58 (1985) 2043.
[38] K. Machida, K. Yoshida, M. Enyo, Y. Toda, T. Masumoto, J. Less-Commun. Met. 119 (1986) 143.
[39] K. Machida, M. Enyo, K. Kai, K. Suzuki, J. Less-Commun. Met. 100 (1984) 377.
[40] K. Machida, M. Enyo, I. Toyoshima, Y. Toda, T. Masumoto, Surf. Coat. Technol. 27 (1986) 359.
[41] G.V. Smith, W.E. Beower, O. Zahraa, A. Molnar, M.M. Khan, B. Rihter, J. Catal. 83 (1983) 238.
[42] B.C. Giessen, S.S. Mahmoud, D.A. Forsyth, M. Hediger, Mater. Sci. Soc. Symp. Proc. 8 (1982) 255.
[43] J. van Wonterghem, S. Morup, C.J.W. Koch, S.W. Charles, S. Wells, Nature (London) 322 (1986) 622.
[44] S. Linderoth, S. Morup, J. Appl. Phys 69 (1991) 5256.
[45] S. Linderoth, S. Morup, S.A. Sethi, Proceedings of NATO Advanced Study Institute on Nano-crystalline Magnetic Materials, 1990, p. 45.
[46] S. Linderoth, S. Morup, C.J.W. Koch, S. Wells, S.W. Charles, J. van Wonterghem, A. Meagher, J. Phys. (Paris) Colloq. 49 (1991) C8.
[47] S. Linderoth, S. Morup, M.D. Bentzon, J. Magn. Magn. Mater. 83 (1990) 457.
[48] S. Wells, S.W. Charles, S. Morup, S. Linderoth, J. van Wonterghem, J. Larsen, M.B. Madsen, J. Phys. 1 (1989) 8199.
[49] S. Linderoth, S. Morup, J. Appl. Phys. 67 (1990) 4472.
[50] S. Linderoth, S. Morup, A. Meagher, J. Larsen, M.D. Bentzon, B.S. Clausen, C.J.W. Koch, S. Wells, S.W. Charles, J. Magn. Magn. Mater. 81 (1989) 138.
[51] H.X. Li, W.J. Wang, J.F. Deng, Chem. Lett. 4 (1998) 371.
[52] J.F. Deng, X.P. Zhang, Appl. Catal. 37 (1988) 339.
[53] J.F. Deng, X.P. Zhang, Solid State Ionics 32 (1989) 1006.
[54] C. Sheng, S. Zhou, H.X. Li, J.F. Deng, Acta Phys.-Chem. Sinica 14 (1998) 164.
[55] B.R. Shen, K.N. Fan, J.F. Deng, Appl. Phys. A 65 (1997) 295.
[56] Z. Hu, J. Shen, Y. Chen, J. Non-Cryst. Solids 159 (1993) 88.

[57] J. Shen, Z. Hu, L. Zhang, Z. Li, Y. Chen, Appl. Phys. Lett. 59 (1991) 3545.
[58] Y. Okamoto, Y. Nitta, T. Lmanaka, S. Teranishi, J. Chem. Soc., Faraday Trans. I 75 (1979) 2027.
[59] W.J. Wang, M.H. Qiao, S.H. Xie, J.F. Deng, Appl. Catal. 167 (1997) 101.
[60] W.J. Wang, M.H. Qiao, H.X. Li, J.F. Deng, Appl. Catal. A. 166 (1998) L243.
[61] W.J. Wang, M.H. Qiao, H.X. Li, J.F. Deng, Appl. Catal. A. 168 (1998) 151.
[62] W.J. Wang, H.X. Li, J.F. Deng, J. Catal., submitted.
[63] N.N. Greenwood, R.V. Parish, P. Thornton, Quart. Rev. 20 (1966) 441.
[64] J.A. Schreifels, P.C. Maybury, W.E. Swartz Jr., J. Catal. 65 (1980) 195.
[65] H.X. Li, H. Li, J.F. Deng, Bull. Sci. China, (1997) in press.
[66] H.X. Li, W.L. Dai, J.F. Deng, Chem. Lett. (1997) 133.
[67] K.D. Ghuge, A.N. Bhat, G.P. Babu, Appl. Catal. 103 (1993) 183.
[68] H.X. Li, H.Y. Chen, J.F. Deng, Appl. Surf. Sci. 25 (1997) 115.
[69] J.S. Yang, S.Z. Dong, H. Li, J.F. Deng, Acta Phys. Sinica 46 (1997) 490.
[70] H.X. Li, Ph.D. Dissertation, Fudan University, (1997).
[71] W.L. Dai, M.H. Qiao, J.F. Deng, Appl. Surf. Sci. 120 (1997) 119.